A surface-enhanced Raman scattering (SERS)-active optical fiber sensor based on a three-dimensional sensing layer

CrossMark

Chunyu Liu [a,b], Shaoyan Wang [a], Gang Chen [a], Shuping Xu [a], Qiong Jia [c], Ji Zhou [d], Weiqing Xu [a,*]

[a] State Key Laboratory of Supramolecular Structure and Materials, Jilin University, Changchun 130012, People's Republic of China
[b] College of Science, Changchun University of Science and Technology, Changchun 130022, People's Republic of China
[c] College of Chemistry, Jilin University, Changchun 130012, People's Republic of China
[d] Hubei Collaborative Innovation Center for Advanced Organic Chemical Materials, Ministry of Education Key Laboratory for the Synthesis and Application of Organic Function Molecules, Hubei University, Wuhan 430062, People's Republic of China

ARTICLE INFO

ABSTRACT

To fabricate a new surface-enhanced Raman scattering (SERS)-active optical fiber sensor, the design and preparation of SERS-active sensing layer is one of important topics. In this study, we fabricated a highly sensitive three-dimensional (3D) SERS-active sensing layer on the optical fiber terminal via *in situ* polymerizing a porous polymer material on a flat optical fiber terminal through thermal-induced process, following with the photochemical silver nanoparticles growth. The polymerized polymer formed a 3D porous structure with the pore size of 0.29–0.81 μm, which were afterward decorated with abundant silver nanoparticles with the size of about 100 nm, allowing for higher SERS enhancement. This SERS-active optical fiber sensor was applied for the determination of 4-mercaptopyridine, crystal violet and maleic acid The enhancement factor of this SERS sensing layer can be reached as about 10^8. The optical fiber sensor with high sensitive SERS-active porous polymer is expected for online analysis and environment detection.

1. Introduction

Surface-enhanced Raman scattering (SERS)-active optical fiber sensors combine the SERS substrate with optical waveguide, which allow the applications for *in situ* and long-distance SERS detections [1–3]. Novel designs of the SERS-active sensing layer is one of the most important subjects in the development of new SERS active optical fiber sensors [4–7]. The quality of sensing layer results in the sensitivity and selectivity of a SERS-active optical fiber sensor. There are many literatures referring to the fabrication techniques of the SERS-active sensing layer on the optical fiber end. Most of them are based on the methods of preparing SERS substrates as references [8–12]. For example, the vacuum deposited Ag islands [8,9], and the assembly of metal colloidal nanoparticles [10]. In

our previous work, we developed a route of the laser-induced metal deposition to *in situ* modify the fiber tip with SERS-active sensing layer [11,12]. This method has the advantages of rapidity (within several minutes) and easy control. It can achieve effective adjustments on nanoparticle size and localized surface plasmon resonance (LSPR) only by the light irradiation time.

To develop SERS-active sensing layers on optical fibers requires solving the same problem as to develop SERS substrates: higher detection sensitivity. To access this purpose, a three-dimensional (3D) porous structure is proposed. The porous structure provides a large surface area, which allows a great deal metal nanoparticles and analytes to posit on [13,14]. More metal nanoparticles supply higher electromagnetic field enhancement, supporting for higher enhancement ability [15–17]. Also, the large surface area of porous structure can enrich target analytes for ultralow concentration analysis.

To achieve this design, we chose a porous polymer named poly(glycidyl metharylate-*co*-ethylene) dimethacrylate (poly (GMA-*co*-EDMA))to modify the optical fiber. Poly (GMA-*co*-EDMA) is a material with microchannels and widely used for preparing porous polymer monoliths for high-performance liquid chromatography [18–23]. After *in situ* thermal polymerization, poly

(GMA-co-EDMA) formed a three-dimensional pore structure on the surface of optical fiber. Then, we employed the laser-induced metal deposition to *in situ* grow Ag nanoparticles on the porous polymer. The fabrication process of the porous polymer was optimized by polymerization temperature and its morphologies were characterized by scanning electron microscope (SEM). This novel SERS-active optical fiber sensor was applied for the SERS determination of 4-mercaptopyridine (4-Mpy) and crystal violet (CV) and the SERS enhancement factor was evaluated.

2. Material and methods

2.1. Materials and instrument

Glycidyl methacrylate (GMA), ethylene glycol dimethacrylate (EDMA), cyclohexanol and 1-dodecanol, 2,2′-azobis(2-methylpropionitrile) (AIBN), 3-(trimethoxysilyl)propyl methacrylate (r-MAPS), 4-mercaptopyridine (4-Mpy, 95%) were purchased from Sigma–Aldrich Co., Ltd. Methanol, silver nitrate, sodium citrate dehydrate, and crystal violet (CV) were obtained from Beijing Chemical Industry. All the chemicals were used without further purification.

Multimode quartz optical fibers (Nanjing Chunhui Science and Technology Industrial Co., Ltd.) used in the experiments have a cladding of 15 μm and a core of 400 μm with the numerical aperture (NA) of 0.37. Ultrapure water was prepared with Milli-Q ultrapure water purification system (18.1 MΩ, Millipore).

A HORIBA T64000 Raman spectrometer fixed with a Spectra-Physics stabilite 2017 argon ion gas laser and a OLYMPUS BX41 microscope with the 10× objective lens (numeral aperture = 0.25) was used for the laser-induced Ag deposition, Raman and SERS

detections. The excitation wavelength was 514.5 nm. The laser powers reaching near and terminal ends were 17.3 and 14.1 mW, respectively. The laser power was measured by a CHERENT laser power meter. All SERS spectrum data were processed with baseline and silica background subtraction.

Scanning electron microscope (SEM, Hitachi New generation Cold Field Emission SEM SU8000 Series, acceleration voltage 5.0 kV) was used to take SEM images.

2.2. Preparation of SERS-active optical fiber

The process of polymerization in deposit end of optical fiber was shown in Scheme 1. Optical fibers were cut into 20 cm length and both ends were grounded with 3000 mesh emery paper for 5 min, 3 μm fiber abrasive sheets for 5 min and 1 μm fiber abrasive sheets for 10 min. After being polished, they were ultrasonically cleaned with ultrapure water, ethanol, and ultrapure water for 10 min and naturally dried. One tip of the cleaned optical fiber (terminal end) was activated by 0.1 M NaOH, 0.1 M HCl, ultrapure water, methanol for 30 min, respectively, and then dried by nitrogen. The 50% (v/v) r-MAPS methanol solution was used to activate the terminal end of fiber. The process of silanization was carried out in a water bath at 45 °C for 12 h.

To synthesize a porous polymer material, a reaction solution containing 24% (w/w) GMA (functional monomer), 16% (w/w) EDMA (cross-linker), 30% (w/w) cyclohexanol, 30% (w/w) 1-dodecanol (porogens), and 1% (w/w) AIBN (with respect to monomers) were prepared. We immersed the terminal end of optical fibers in above reaction solution. The polymerization of GMA-co-EDMA was carried out in a water bath at different heating temperatures (60, 65, 70 and 75 °C). After the polymerization reaction was
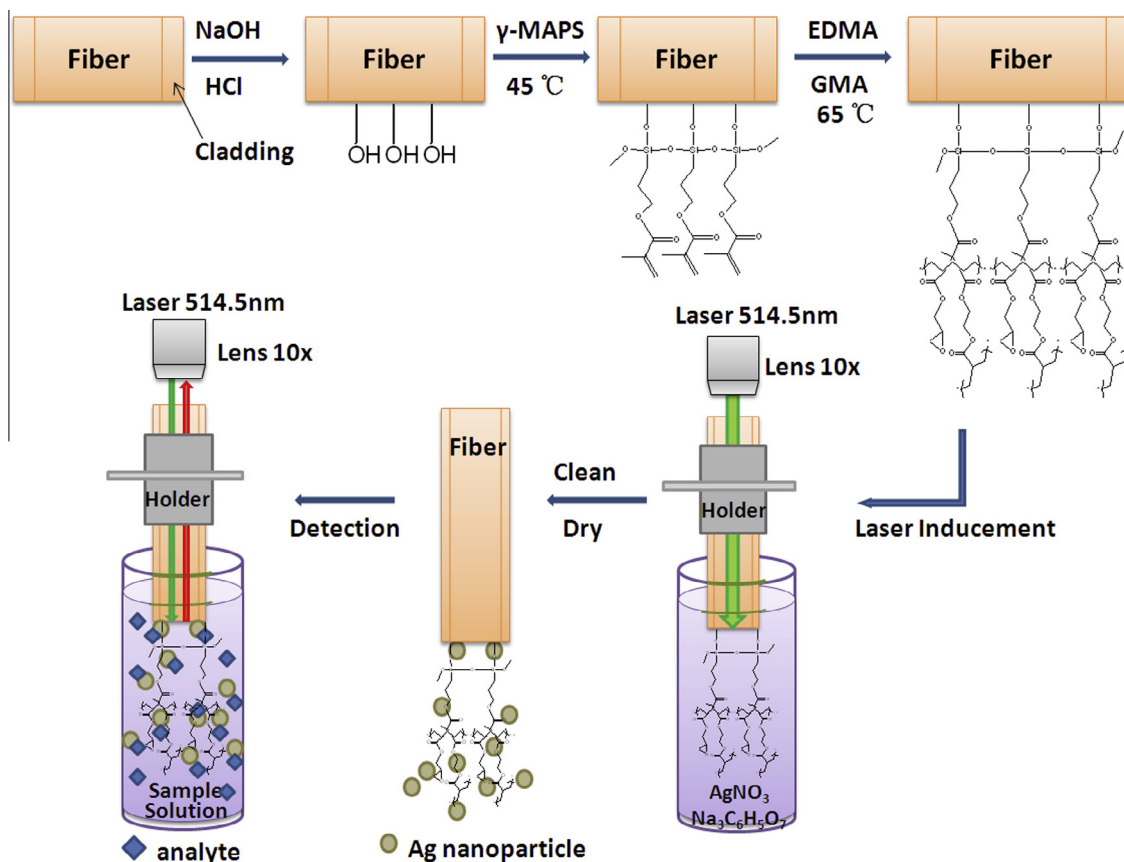
Scheme 1. Preparation of a SERS-active sensing layer on the terminal end of an optical fiber and its application for SERS detection.
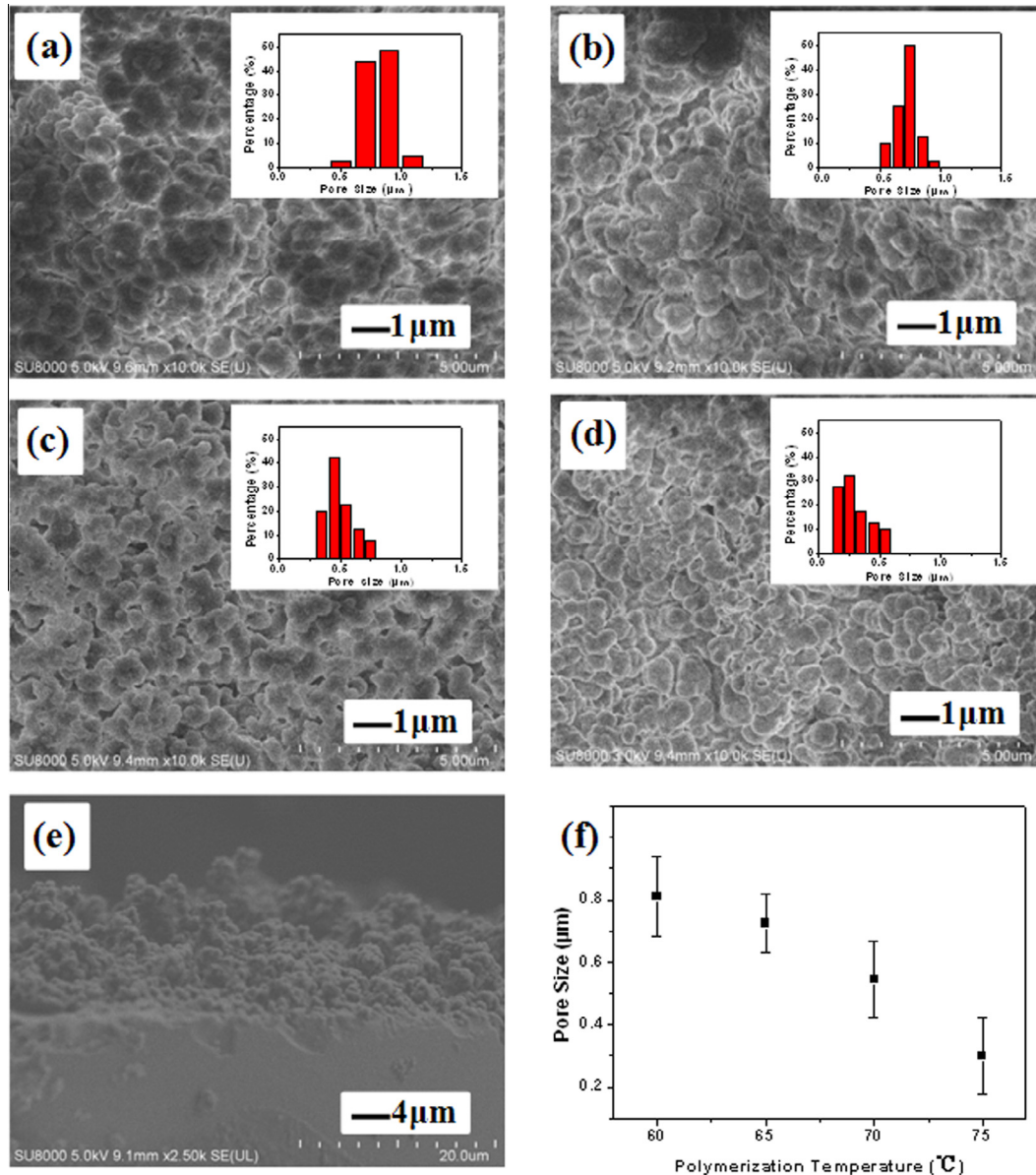
Fig. 1. (a)–(d) are the SEM images of the poly (GMA-*co*-EDMA) porous polymer in the terminal end of optical fibers under the polymerization temperatures of 60, 65, 70 and 75 °C, respectively. Insets are the pore size distribution. (e) SEM image of the side view of SERS-active optical fiber. The polymerization temperature was 65 °C. (f) The plots of the pore size vs. polymerization temperature.

completed, optical fibers were dipped into methanol for 8 h and ultrapure water for 15 min to remove unreacted components.

For the laser-inducement reduction of Ag on the porous structure, a silver growth solution containing 1 mL of silver nitrate (1.0×10^{-2} M) and 1 mL of trisodium citrate (1.0×10^{-2} M) was prepared first [11,12]. The silver growth solution was kept away from light before use. One end of the optical fiber was exposed to a 514.5 nm laser (the power reaching sample was 17.3 mW) for focusing the laser to optical fiber (see Scheme 1). The other terminal end with the laser power of 14.1 mW was immersed into the silver growth solution for the light-induced reduction of Ag nanoparticles. The irradiation experienced several minutes. After that, the optical fiber with the SERS-active sensing layer was cleaned with water and dried before use.

2.3. SERS detection by SERS optical fiber sensor

To measure SERS spectra of analytes, the 514.5 nm laser was focused on the near end of the optical fiber. The light passed

through the fiber and the decorated polymer layer and then exposed from the terminal end. The SERS optical fiber sensor we used for SERS detection was prepared by the optimization conditions as 65 °C thermal polymerization and 5 min laser-induced Ag deposition. The terminal end was immersed into a probed solution. The laser light resonant with the LSPR of Ag nanoparticles on the terminal end, further excited analytes, emitting SERS signal. The Raman scattering of the analytes would then be collected by the same terminal end of the optical fiber and further transmitted to the other end, finally recorded by a spectrometer (HORIBA T64000 Raman spectrometer).

3. Results and discussion

3.1. The optimization of polymerization temperature for pore size

The pore structure of porous materials is affected by many factors, such as the polymerization reaction time, temperature, the

ratio of reaction solutions, and so on [18–23]. In the present study, we adopted the polymerization temperature to control pores formed on the terminal end of optical fibers. Fig. 1 shows the SEM images of poly(GMA-co-EDMA) porous polymer in the terminal end of optical fibers under different heating temperatures. As can be seen from the figure, the thermal polymerization of porous material grew uniform on the optical fiber tip, forming a dense 3D pore structure. The particle size distributions (see the insets of Fig. 1) show the average size of polymer particles are 0.65, 0.51, 0.47 and 0.45 μm for 60, 65, 70 and 75 °C polymerization, respectively, presenting a decreasing trend with polymerization temperature. Apparently, larger particle size results in larger pore size in space. The statistical results from SEM images show the average pore size are 0.81, 0.71, 0.54 and 0.29 μm for Fig. 1a–d, respectively. The side view displays the porous polymer on the terminal end is uniform. The thickness is in the range of 11.4–6.7 μm and the average thickness is about 8.6 μm.

The morphology of the porous polymer particle influences in the light-induced growth of Ag nanoparticles, and further SERS enhancement ability. So, we optimized the porous polymer particles by SERS intensity. We modified Ag nanoparticles by laser-induced reduction reaction on the poly(GMA-co-EDMA) porous polymer with different pore sizes, which had been prepared under different polymerization temperatures. The irradiation time for Ag growth was kept at 4.0 min for all trials. Fig. 2(a) shows the SERS spectra of 4-Mpy (1.0×10^{-4} M) via the SERS-active optical fibers with different polymer pore sizes fabricated under different polymerization temperatures. Fig. 2(b) plots the 4-Mpy SERS intensity at 1578 cm^{-1} vs. pore size of porous polymers. It can be observed the relatively stronger SERS intensities were obtained on the porous polymers prepared under 65–70 °C. This indicates that too large pore size causes the lower surface area of 3D porous structure, which is disadvantageous to the loading of Ag nanoparticles and further SERS enhancement. However, too small pore size is also against the SERS enhancement due to the low diffusion mobility for both Ag growth solution and probed molecules.

3.2. The optimization of light irradiation time for Ag nanoparticles formation

According to our previous study [11,12] and the research of Yang et al. [24,25], the irradiation time in laser-induced Ag growth method dominates the metal particle size, further affects the LSPR properties of SERS-active layer and its SERS enhancement as well. In this study, we chose trisodium citrate (1.0×10^{-2} M) and AgNO$_3$ (1.0×10^{-2} M) as the Ag growth solution to optimize the irradiation time. Fig. 3(a) displays the SERS spectra of 4-Mpy (1.0×10^{-4} M) with the SERS-active optical fibers fabricated under different irradiation time for silver nanoparticles growth. Fig. 3(b) plots the SERS intensity vs. irradiation time. From the figure it can be clearly observed that the SERS intensity of 4-Mpy experiences an increase and then a decrease with the irradiation time. The highest SERS was observed when the irradiation time was 4–5 min. Too little irradiation time causes the formation of few Ag nanoparticles, leading to low SERS enhancement. Too long time irradiation produces very thick silver deposition, causing strong absorption for SERS signal of probes. For the further study, we chose 4 min for laser-induced Ag reduction.

Fig. 4(a) and (b) show the morphologies of the porous polymers with Ag nanoparticles. It can be found that there are a great number of Ag nanoparticles formed on the porous polymer material, having a size of about 80–100 nm. They are dense and uniform, which is favourable for forming Ag nanoaggregates and "hot spots", supporting tremendous electromagnetic field enhancement for SERS. In addition, the porous structure allows
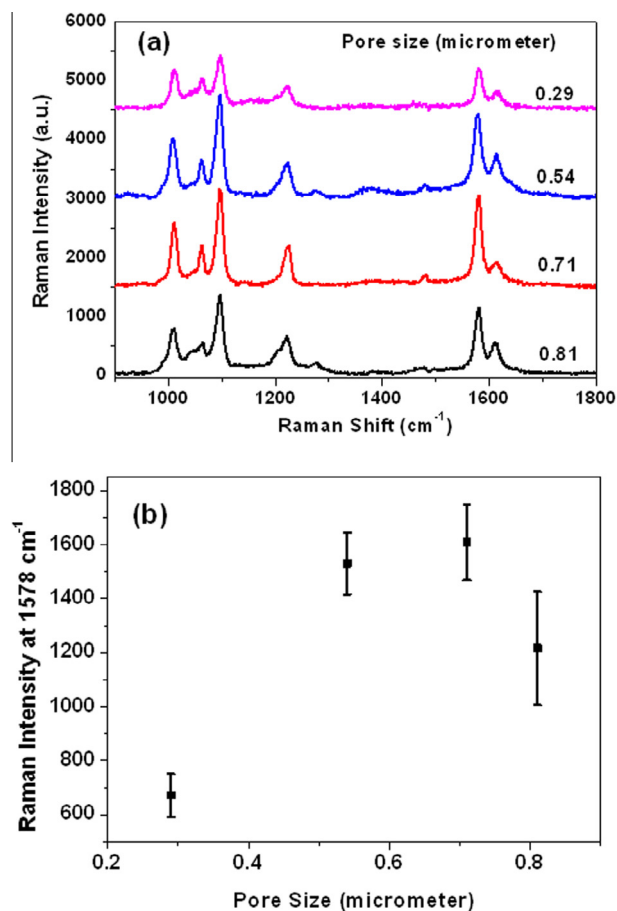

Fig. 2. (a) SERS spectra of 4-Mpy (1.0×10^{-4} M) obtained by using different SERS-active optical fibers with different polymer pore sizes fabricated under different polymerization temperatures (60, 65, 70 and 75 °C). (b) The SERS intensity of 4-Mpy at 1578 cm^{-1} vs. the pore size of porous polymers.

the analytes to access the Ag nanoparticles, which is helpful for improving SERS signal.

### 3.3. Enhancement ability of SERS-active sensing layer

To evaluate the enhancement ability of the as-prepared SERS-active optical fiber, we calculated the enhancement factor (G) by comparing the SERS signal obtained by the SERS-active optical fiber with normal Raman signal obtained a naked multimode optical fiber. The calculation is according to the method reported by Gupta and Weimeras [26]:

$$G = \frac{I_{SERS}/N_{SERS}}{I_{Raman}/N_{Raman}} \qquad (1)$$

where N_{Raman} and N_{SERS} denote the number of probe molecules which contribute to the signal intensity, normal and enhanced, respectively. I_{Raman} and I_{SERS} denote the corresponding normal Raman and SERS intensity. In our experiment, because the 4-Mpy adsorbed onto the sliver is a monolayer, the enhancement factor can be written in the following form:

$$G = \frac{I_{SERS}}{A \times \frac{M_{SERS}}{S_{SERS}}} \times \frac{A \times \frac{M_{RAMAN}}{S_{RAMAN}}}{I_{RAMAN}} \qquad (2)$$

where S_{SERS} and S_{Raman} is the geometrical area of 4-Mpy casting film on the surface of SERS-active optical fiber and normal multimode optical fiber. Since we used the same kind of optical fiber in this
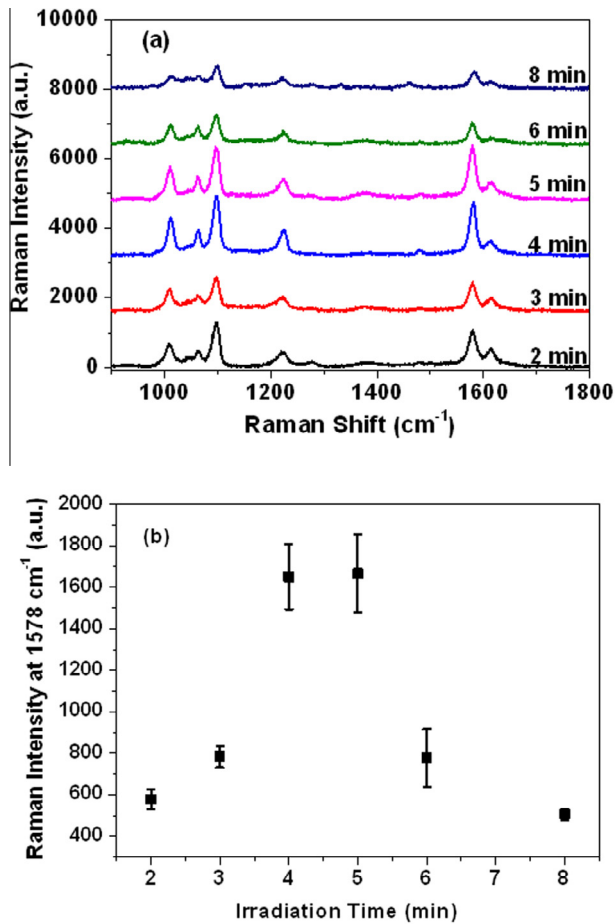
Fig. 3. (a) SERS spectra of 4-Mpy (1.0×10^{-4} M) with different SERS-active optical fibers prepared under different laser irradiation time (2, 3, 4, 5, 6 and 8 min) for Ag deposition. (b) SERS intensity of 4-Mpy at 1578 cm^{-1} vs. the irradiation time of Ag deposition.

Fig. 4. SEM micrograph of the structure of the poly (GMA-co-EDMA) porous polymer in the terminal end of the cleaned optical fiber after laser induced 4 min with different polymerization temperature 65 °C (a) and 70 °C (b).
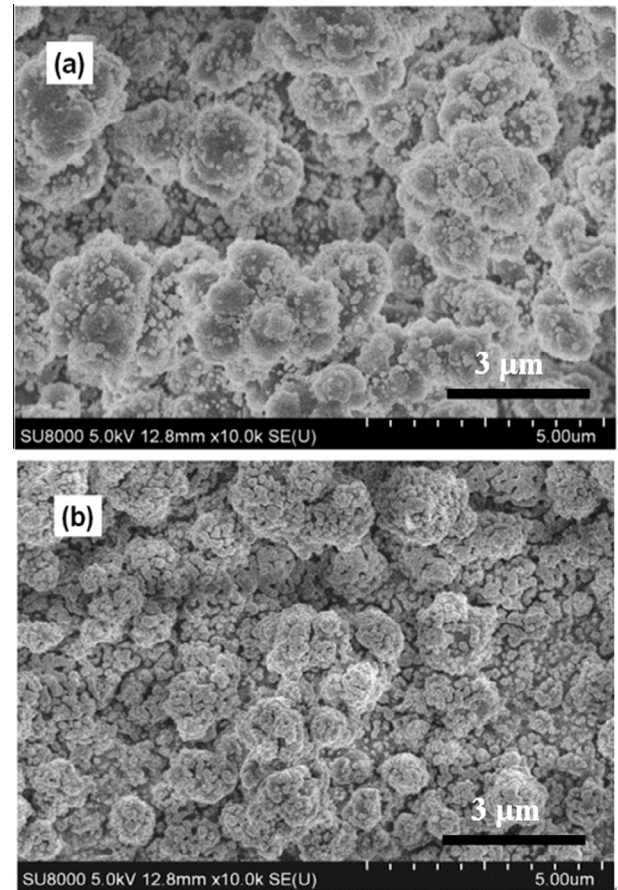
experiment, the contact surface area was uniform between tip of optical fiber and the sample solution. So S_{SERS} is as same as S_{Raman}. A is the recorded area of the laser spot. The laser spot area of normal Raman is same as that of SERS. The SERS signal (I_{SERS}) and the normal Raman signal (I_{Raman}) were measured at the same laser power, incident angle (180°) and the same type of multimode optical fiber. The representative band at 1578 cm^{-1} (the band is 1591 cm^{-1} in normal Raman) was selected to calculate the enhancement factor values. The SERS signal intensity at 1578 cm^{-1} is 823.1 cps and normal Raman signal intensity at 1591 cm^{-1} is 43.6 cps (Fig. 5). M_{SERS} and M_{Raman} are the number of 4-Mpy molecules adsorbed on silver film of the surface of SERS-active optical fiber and normal multimode optical fiber. M can be calculated by Eq. (3).

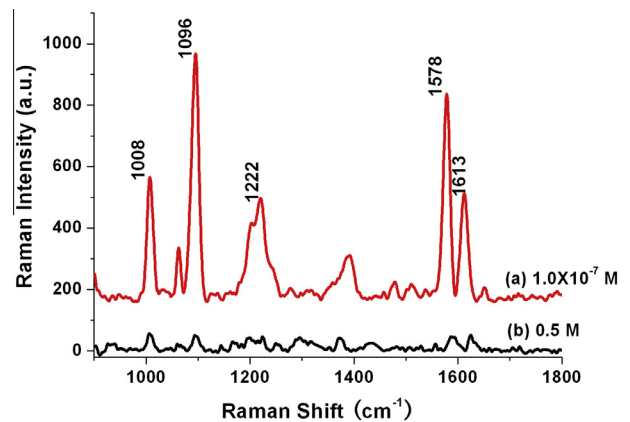$$M = c_{4\text{-Mpy}} \times V \times N_A \qquad (3)$$

Here, $c_{4\text{-Mpy}}$ is the concentration of 4-Mpy. The volume of 4-Mpy presents as V. N_A is the Avogadro's constant. Thus, the value of G is equal to 9.4×10^7. This G value is 100 times higher over the scientific standards of a SERS substrate in which the bulk G in excess of 10^5 is desired [27].

3.4. Concentration-dependant SERS detections

To measure SERS spectra of probes, the laser was focused on one end of the optical fiber and propagated within the fiber. The terminal end was immersed into a probed solution (Scheme 1) for an in situ detection. The laser light interacts with the LSPR of Ag

Fig. 5. (a) The SERS spectrum of 4-Mpy (1.0×10^{-7} M) measured with the SERS-active optical fiber. (b) Normal Raman spectrum of 4-Mpy (0.5 M) measured with an optical fiber. The integrate time are 50 s for both.

nanoparticles on the terminal end, further enhanced the Raman signal of probes. The Raman scattering signal was collected by the optical fiber and propagated to the other end, finally recorded by the Raman instrument. Fig. 6 shows the concentration-dependant SERS detections of 4-Mpy, crystal violet and maleic acid (a type of illegal food additive) with the SERS-active optical fibers. It should be noted that the Raman band background of the optical fiber all appears in the range lower than 1000 cm^{-1}. It would not bother the Raman measurements of most phenyl and aromatic
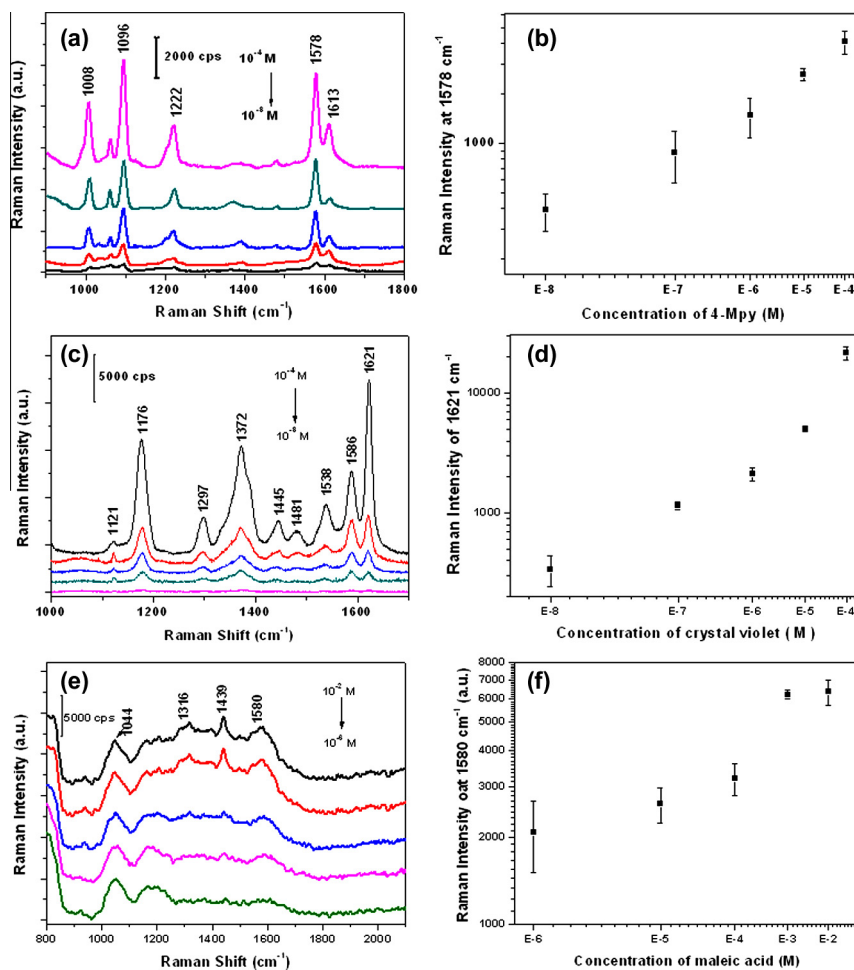
Fig. 6. SERS spectra of 4-Mpy (a), crystal violet (c) and maleic acid (e) under different concentrations probed by using the SERS-active optical fibers. The concentrations from top to bottom are 1.0×10^{-4} to 1.0×10^{-8} M in (a) and (c) and 1.0×10^{-2} to 1.0×10^{-6} M in (e). (b), (d) and (f) are the plots of SERS intensities at 1578 cm^{-1} for 4-Mpy, 1621 cm^{-1} for crystal violet and 1580 cm^{-1} for maleic acid vs. probed concentrations.

compounds. Fig. 6(b), (d) and (f) are the working curves for *in situ* SERS detections of 4-Mpy, crystal violet and maleic acid, respectively. The results show that the lowest detection concentrations are 1.0×10^{-7} M for 4-Mpy and crystal violet and 1.0×10^{-5} M for maleic acid.

It can be found that the SERS signal of a 4-Mpy solution when the 1.0×10^{-7} M is much lower than that in Fig. 5. The difference comes from the sample loading ways. Fig. 6 has been achieved by the *in situ* SERS detections. However, for the G value calculation, we adopted the casting film for sample loading, which is a concentrated and accumulated process of samples on the 3D porous structure and supposed to have a higher sample density far away from 1.0×10^{-7} M. It also indicates that this detection limit of this SERS sensor could be much more lower (possibly 10^{-8} M) if we measure samples using casting films.

4. Conclusions

We developed a novel SERS-active optical fiber based on the design of 3D pore structure enriched with Ag nanoparticles. The *in situ* thermal-polymerized GMA-*co*-EDMA formed a quasi-spherical porous structure with the pore size of 0.29–0.81 μm. Via the laser-induced Ag growth method, Ag nanoparticles formed on the polymer surface. The high loading and close-packing of Ag nanoparticles allow a great many of SERS "hot spots", supporting for higher SERS detection sensitivity. This SERS-active optical fiber

can be widely applied for the determination of analytes in liquid solutions. This fabrication for SERS-active sensing layer is easy and controllable. The obtained SERS-active optical fiber has acceptable detection sensitivity. We expect this *in situ* preparation route can be extended to fabricate many optical devices which require enlarged surface area. Also, this SERS-active optical fiber can be employed for many fields, for example, SERS monitoring of contaminations in surrounding water.

Conflict of interest

We declared that we have no conflicts of interest to this work.

Acknowledgments

References

[1] X.D. Wang, O.S. Wolfbeis, Fiber-optic chemical sensors and biosensors, Anal. Chem. 85 (2013) 487–508.

[2] S.M. Borisov, O.S. Wolfbeis, Optical biosensors, Chem. Rev. 108 (2008) 423–461.

[3] G. Brambilla, Optical fibre nanotaper sensors, Opt. Fiber Technol. 16 (2010) 331–342.

[4] J.M. Bello, V.A. Narayanan, D.L. Stokes, T. Vo-Dinh, Fiber-optic remote sensor for in situ surface-enhanced Raman scattering analysis, Anal. Chem. 62 (1990) 2437–2441.

[5] K.I. Mullen, K.T. Carron, Surface-enhanced Raman spectroscopy with abrasively modified fiber optic probes, Anal. Chem. 63 (1991) 2196–2199.

[6] A. Pesapane, A. Lucotti, G. Zerbi, Fiber-optic SERS sensor with optimized geometry: testing and iptimization, J. Raman Spectrosc. 41 (2010) 256–267.

[7] D.L. Stokes, T. Vo-Dinh, Development of an integrated single-fiber SERS sensor, Sensor. Actuat. B Chem. 69 (2000) 28–36.

[8] C. Viets, W. Hill, Comparison of fibre-optic SERS sensors with differently prepared tips, Sens. Actuat. B 51 (1) (1998) 92–99.

[9] W.Q. Xu, S.P. Xu, B. Hu, K.X. Wang, Y.T. Xie, Y.G. Fan, Studies on the SERS-active optic fiber probe, Chem. J. Chinese U. 25 (2004) 114–117.

[10] W.Q. Xu, S.P. Xu, Z.C. Lü, K.X. Wang, B. Zhao, Y.G. Fang, Preparation of SERS-active liquid core fiber and its application to the ultrasensitive detection, Chem. J. Chinese Univ. 11 (2003) 2083–2085.

[11] X.L. Zheng, D.W. Guo, Y.L. Shao, S.J. Jia, S.P. Xu, B. Zhao, W.Q. Xu, Photochemical modification of an optical fiber tip with a silver nanoparticle film: a SERS chemical sensor, Langmuir 24 (2008) 4394–4398.

[12] S.J. Jia, S.P. Xu, X.L. Zheng, B. Zhao, W.Q. Xu, Preparation of SERS optical fiber sensor via laser-induced deposition of Ag film on the surface of fiber tip, Chem. J. Chinese Univ. 27 (2006) 523–526.

[13] Q. Cao, Y. Xu, F. Liu, F. Svec, M.J. Fréchet, Polymer monoliths with exchangeable chemistries: use of gold nanoparticles as intermediate ligands for capillary columns with varying surface functionalities, Anal. Chem. 82 (2010) 7416–7421.

[14] Y. Lv, F.M. Alejandro, M.J. Fréchet, F. Svec, Preparation of porous polymer monoliths featuring enhanced surface coverage with gold nanoparticles, J. Chromatogr. A. 1261 (2012) 121–128.

[15] J.K. Liu, I. White, D.L. Devoe, Nanoparticle-functionalized porous polymer monolith detection elements for surface-enhanced Raman scattering, Anal. Chem. 83 (2011) 2119–2124.

[16] Q.Q. Li, Y.P. Du, H.R. Tang, X. Wang, G.P. Chen, J. Iqbal, W.M. Wang, W.B. Zhang, Ultra sensitive surface-enhanced Raman scattering detection based on monolithic column as a new type substrate, J. Raman Spectrosc. 43 (2012) 1392–1396.

[17] C. Liu, Q. Jiang, L. Chen, H. Zhang, H.-X. Chen, J. Zhou, Y. Ye, Ultrasensitive surface-enhanced Raman scattering detection with nanoparticle-functionalized amino silica monolith, Chem. J. Chinese Univ. 34 (2013) 2488–2492.

[18] E.C. Peters, F. Svec, J.M.J. Frechet, Rigid macroporous polymer monoliths, Adv. Mater. 11 (1999) 1169–1181.

[19] D.S. Peterson, T. Rohr, F. Svec, J.M. Frechet, Enzymatic microreactor-on-a-chip: protein mapping using trypsin immobilized on porous polymer monoliths molded in channels of microfluidic devices, J. Anal. Chem. 74 (2002) 4081–4088.

[20] T. Rohr, C. Yu, M.H. Davey, F. Svec, J.M. Frechet, Porous polymer monoliths: simple and efficient mixers prepared by direct polymerization in the channels of microfluidic chips, J. Electrophoresis 22 (2001) 3959–3967.

[21] J. Liu, C.F. Chen, C.C. Chang, C.C. Chu, D.L. DeVoe, Polymer microchips integrating solid-phase extraction and high-performance liquid chromatography using reversed-phase polymethacrylate monoliths, Anal. Chem. 81 (2009) 2545–2554.

[22] F. Svec, Porous polymer monoliths: amazingly wide variety of techniques enabling their preparation, J. Chromatogr. A. 1217 (2010) 902–924.

[23] Z. Walsh, S. Abele, B. Lawless, D. Heger, P. Klán, M.C. Breadmore, B. Paull, M. Macka, Photoinitiated polymerization of monolithic stationary phases in polymide coated capillaries using visible region LEDs, Chem. Commun. 48 (2008) 6504–6506.

[24] T. Liu, X. Xiao, C.X. Yang, Surfactantless photochemical deposition of gold nanoparticles on an optical fiber core for surface-enhanced Raman scattering, Langmuir 27 (2011) 4623–4626.

[25] M.S. Li, C.X. Yang, Laser-induced silver nanoparticles deposited on optical fiber core for surface-enhanced Raman scattering, Chinese Phys. Lett. 27 (2010) 044202.

[26] R. Gupta, W.A. Weimer, High enhancement factor gold films for surface enhanced Raman spectroscopy, Chem. Phys. Lett. 374 (2003) 302–306.

[27] M.J. Natan, Concluding remarks surface enhanced Raman scattering, Faraday Discuss. 132 (2006) 321–328.